Neurosci. Bull. March, 2020, 36(3):202–216
https://doi.org/10.1007/s12264-019-00423-3

www.neurosci.cn
www.springer.com/12264

ORIGINAL ARTICLE

Rabies Virus Pseudotyped with CVS-N2C Glycoprotein as a Powerful Tool for Retrograde Neuronal Network Tracing

Xutao Zhu[1,2,6] · Kunzhang Lin[3] · Qing Liu[2] · Xinpei Yue[2] · Huijie Mi[4] · Xiaoping Huang[2] · Xiaobin He[2] · Ruiqi Wu[2] · Danhao Zheng[4] · Dong Wei[4] · Liangliang Jia[2] · Weilin Wang[4] · Anne Manyande[5] · Jie Wang[2] · Zhijian Zhang[2] · Fuqiang Xu[1,2,3]

Received: 2 February 2019 / Accepted: 17 June 2019 / Published online: 23 August 2019

Abstract Efficient viral vectors for mapping and manipulating long-projection neuronal circuits are crucial in structural and functional studies of the brain. The SAD strain rabies virus with the glycoprotein gene deleted pseudotyped with the N2C glycoprotein (SAD-RV(ΔG)-N2C(G)) shows strong neuro-tropism in cell culture, but its *in vivo* efficiency for retrograde gene transduction and neuro-tropism have not been systematically characterized. We compared these features in different mouse brain regions for SAD-RV-N2C(G) and two other widely-used retrograde tracers, SAD-RV(ΔG)-B19(G) and rAAV2-retro. We found that SAD-RV(ΔG)-N2C(G) enhanced the infection efficiency of long-projecting neurons by ~10 times but with very similar neuro-tropism, compared with SAD-RV(ΔG)-B19(G). On the other hand, SAD-RV(ΔG)-N2C(G) had an infection efficiency comparable with rAAV2-retro, but a more restricted diffusion range, and broader tropism to different types and regions of long-projecting neuronal populations. These results demonstrate that SAD-RV(ΔG)-N2C(G) can serve as an effective retrograde vector for studying neuronal circuits.

Keywords Viral vector · N2C glycoprotein · Neuronal circuits · Retrograde tracing

Introduction

In the central nervous system, distinct brain regions work together through particular circuit connections to process different and complex information [1–7]. Neuronal circuits are the keystone to brain functions and their anatomical and

Electronic supplementary material The online version of this article (https://doi.org/10.1007/s12264-019-00423-3) contains supplementary material, which is available to authorized users.

✉ Zhijian Zhang
zhzhj_hust@126.com

✉ Fuqiang Xu
fuqiang.xu@wipm.ac.cn

[1] Shenzhen Key Lab of Neuropsychiatric Modulation and Collaborative Innovation Center for Brain Science, Guangdong Provincial Key Laboratory of Brain Connectome and Behavior, CAS Center for Excellence in Brain Science and Intelligence Technology, Brain Cognition and Brain Disease Institute (BCBDI), Shenzhen Institutes of Advanced Technology, Chinese Academy of Sciences, Shenzhen-Hong Kong Institute of Brain Science-Shenzhen Fundamental Research Institutions, Shenzhen 518055, China

[2] State Key Laboratory of Magnetic Resonance and Atomic and Molecular Physics, Key Laboratory of Magnetic Resonance in Biological Systems, Wuhan Center for Magnetic Resonance, Wuhan Institute of Physics and Mathematics, Chinese Academy of Sciences, Wuhan 430071, China

[3] Wuhan National Laboratory for Optoelectronics, Huazhong University of Science and Technology, Wuhan 430071, China

[4] College of Life Sciences, Wuhan University, Wuhan 430071, China

[5] School of Human and Social Sciences, University of West London, London, UK

[6] University of the Chinese Academy of Sciences, Beijing 100049, China

functional aberrations are closely associated with many neurodegenerative diseases [8–11], such as Parkinson's disease [12, 13], Alzheimer's disease [14] and Huntington's disease [15]. Thus, it is critical to develop efficient tools for anatomical mapping and the functional decoding of neuronal circuit connections.

Retrograde tracers, owing to their unique properties of entry at axon terminals and then being transported to the cell bodies, are useful tools for targeting the long-projecting neuronal circuit assemblies [16, 17]. Compared with the classical chemical tracers [18–22], viral vectors are able to deliver genetic elements to neuronal populations with specific projection properties or molecular features, and hence are superior in morphological visualization, activity monitoring, and functional modulation in neuroscience studies. Nowadays, viral tools are drawing close attention from the field of neuroscience. The rabies virus (RABV) [23–26], herpes simplex virus (HSV) [27–31], canine adeno virus-2 (CAV-2) [32–34], retrograde adeno-associated virus (rAAV2-retro) [35], and RABV glycoprotein-enveloped lentivirus (LV) [36–38] are among the most commonly-used recent retrograde viral vectors. They seem to have rather different infection efficacies and tropisms, although this has not yet been thoroughly explored. RABV and HSV have broader tropism for different types of neurons [29, 39], and much higher cytotoxicity than CAV-2 and rAAV2-retro. CAV-2 and rAAV2-retro are valuable due to their low toxicity and outstanding retrograde gene transduction efficiency, but are limited by the gene delivery capacity and heterogeneous tropism in different neurons [40, 41]. LV also has high retrograde gene transduction efficiency, but may induce immune responses [42] or tumorigenesis[43]. By far, RABV is reported to ensure robust gene expression, possesses the most exclusive neuro-tropism and the broadest range of host species among the above viruses, but is limited by its cytotoxicity and retrograde gene transduction efficiency. Recent studies have successfully attenuated [44] and even eliminated [40] the cytotoxicity. Moreover, RABV enveloped with the N2C glycoprotein (N2C(G)) from the Challenge Virus Strain displays increased neuro-tropism in cell culture [45] and trans-synaptic efficiency *in vivo* [46]. These improvements endow the RABV-N2C(G) with great potential in both structural and functional studies of neuronal circuits. However, since the cellular environment and receptors involved may be different, the higher *in vitro* neuro-tropism and *in vivo* trans-synaptic spread efficiency do not mean higher retrograde infection efficiency. Thus, the *in vivo* retrograde gene transduction efficiency and tropisms of the RABV enveloped by N2C(G) to long-projecting neuronal circuits and comparison with the two outstanding retrograde tracers (SAD strain RABV and rAAV2-retro) are still unknown.

To address these questions, in this study, we first enveloped the glycoprotein gene-deleted SAD-RABV with N2C(G) (SAD-RV(ΔG)-N2C(G)) or the native glycoprotein (SAD-RV(ΔG)-B19(G)), and then compared the *in vivo* retrograde infection properties of the SAD-RV(ΔG)-N2C(G) with those of SAD-RV(ΔG)-B19(G) and rAAV2-retro.

Methods

Animals

All surgical and experimental procedures were conducted in accordance with the guidelines of the Animal Care and Use Committees (20170712015) at the Wuhan Institute of Physics and Mathematics, Chinese Academy of Sciences. Adult male C57BL/6 mice were purchased from Hunan SJA Laboratory Animal Company. Glutamate decarboxylase 67 (GAD67)-GFP transgenic mice [47] were gifts from Professor Shumin Duan (Zhejiang University), and bred with adult female C57BL/6 mice. All animals were fed *ad libitum* with food and water. A dedicated room with a 12/12 h light/dark cycle was used to house the animals.

Virus Information

The viral vectors SAD-RV(ΔG)-B19(G)-EGFP, SAD-RV(ΔG)-N2C(G)-EGFP, SAD-RV(ΔG)-N2C(G)-mCherry, rAAV2-retro-EF1α-EYFP, and rAAV2-retro-EF1α-mCherry were all packaged by BrainVTA Co., Ltd. (Wuhan, China) and aliquots were stored at −80 °C.

Production of BHK-N2C(G) Cells

For the baby hamster kidney (BHK)-N2C(G) cell lines, FUGW-H2B-GFP-P2A-N2C(G) was created by inserting the N2C-glycoprotein gene (Addgene, #73476) with histone GFP into the lentivirus expression vector FUGW (Addgene, #14883), then transfection into lentiviral packaging cells. After filtration, FUGW-H2B-GFP-P2A-N2C(G) was used to infect BHK cells.

Packaging of the SAD-RV(ΔG)-N2C(G)-EGFP

The SAD-RV(ΔG)-B19(G)-EGFP was packaged using standard methods as described in previous reports [48]. BHK-N2C(G) cells were used to stably express N2C(G) for packaging SAD-RV(ΔG)-N2C(G)-EGFP. The SAD-RV(ΔG)-B19(G)-EGFP was used to infect BHK-N2C(G) cells for 48 h. Then, after collecting viral supernatant, the BHK-N2C(G) cells were washed with PBS, digested with pancreatin, and amplified. After 48 h,

the viral supernatant of SAD-RV(ΔG)-N2C(G)-EGFP was collected, filtered (0.45 μm) and stored at −80 °C. The concentration procedure of SAD-RV(ΔG)-N2C(G)-EGFP was as previously reported [48].

SAD-RV(ΔG)-N2C(G)-mCherry was obtained using the same procedures as for SAD-RV(ΔG)-N2C(G)-EGFP. HEK 293T cells were used to assay the titer of all rabies viruses using limiting dilution analysis. Then the rabies viruses were stored at −80 °C. The rAAV2-retro-EF1α-EYFP and rAAV2-retro-EF1α-mCherry were titrated using QPCR.

Stereotaxic Surgery

The animals were anesthetized with chloral hydrate (400 mg/kg), and placed in a stereotaxic apparatus (RWD, 68030, Shenzhen, China). The skull above the targeted areas was thinned with a dental drill (STRONG, Guangdong, China) and removed carefully with a curved needle. A mixture of virus and Alexa Fluor 594 conjugated-cholera toxin B subunit (CTB594, Thermo Fisher Scientific, C34777; final concentration, 0.02 mg/mL) was injected into the target brain regions (ventral tegmental area (VTA): A-P, −3.10 mm; M-L, ±0.50 mm, D-V, −4.50 mm, 200 nL; or dentate gyrus (DG): A-P, −1.70 mm; M-L, −0.90 mm; D-V, −1.95 mm, 100 nL) using an injector connected to a glass micropipette (WPI, 4878, Sarasota, FL), and driven by a syringe pump (Stoelting, Quintessential Stereotaxic Injector, 53311, Wood Dale, IL). After injection, the micropipette was left in place for 10 min to minimize diffusion and then slowly withdrawn.

Finally, after suturing and applying lidocaine hydrochloride to the wound, the animals were returned to the housing room.

Slice Preparation and Confocal Imaging

Mice were anesthetized with an overdose of chloral hydrate (600 mg/kg), and perfused transcardially with phosphate-buffered saline (PBS) followed by 4% paraformaldehyde (PFA, Sigma, 158127MSDS, St. Louis, MO). The brain was removed and post-fixed overnight in 4% PFA at 4 °C, then coronal sections were cut at 40 μm on a cryostat microtome (Thermo Fisher, NX50, Waltham, MA).

Every sixth section was stained with 4′,6-diamidino-2-phenylindole (DAPI), mounted in 70% glycerol, and imaged under a confocal microscope (Leica, TCS SP8, Buffalo Grove, IL) or a virtual microscopy slide-scanning system (Olympus, VS 120, Tokyo, Japan).

Immunohistochemistry

The sections were washed with PBS (3 times, 5 min each), then incubated in blocking solution (10% normal goat serum and 0.3% Triton x-100 in PBS) for 1 h at 37 °C, followed by the primary antibody rabbit anti-Ca^{2+}/calmodulin-dependent protein kinase II (CaMKII, Abcam, ab5683, 1:500) and incubated for 72 h at 4 °C. Sections were washed with PBS (3 times, 10 min each), incubated with the secondary antibody goat anti-rabbit cy3 (Jackson ImmunoResearch, 94600, 1:400) for 1 h at 37 °C, then washed with PBS (3 times, 10 min each), stained with DAPI, and mounted with 70% glycerol.

Data Analysis

Cell Counting

To count the labeled neurons in the whole brain using SAD-RV(ΔG)-B19(G), SAD-RV(ΔG)-N2C(G), or rAAV2-retro, images were segmented and delineated to different brain regions with Photoshop based on the Allen Brain Atlas (http://www.brain-map.org/). The labeled neurons were quantified with ImageJ (National Institutes of Health, Bethesda, MD), but those around the injection sites were not counted.

To count CaMKII and EYFP/GFP co-labeled cells, 1024 × 1024 pixel (1183 μm × 1183 μm) images within the target regions were randomly selected, while to count GAD 67 or GAD 67-GFP co-labeled cells, the images were segmented and assigned to different brain regions with Photoshop based on the Allen Brain Atlas. The co-labeled neurons were quantified with ImageJ.

Analysis of Viral Diffusion Range

To analyze the diffusion ranges of rAAV2-retro and SAD-RV(ΔG)-N2C(G), we selected samples from around the VTA injection site containing a large enough (2235 μm × 2235 μm) area (referred to as cholera toxin B subunit signals). Since viral diffusion is concentric, the diffusion range was defined as an irregular circle centered on the CTB signals and containing concentric EYFP/GFP+ soma distributions. Only the EYFP/GFP+ signals within the circle were assessed. The circular range was equidistantly segmented into 57.5-μm stripes centered on the CTB signals along the lateral-medial and dorsal-ventral axes using MatLab R (2014a). The EYFP/GFP+ signals within each square were counted and calculated separately.

Statistical Analyses

To illustrate the input intensity from different brain regions, only those >1% were included in Fig. 3D and Fig. S2. For statistical analysis of the input intensity for the whole brain, all regions were included. For diffusion area analysis, the percentage of signal in each square was calculated, fitted to a Gaussian curve, and the $W_{h/2}$ (peak width at half-height) was analyzed using MatLab R (2014a).

Informations on the sections included in each statistical analysis are listed below. About 36 sections from each mouse were included in Figs. 1D, 2B, 3D–E, and S2A–B; ~33 in Fig. 4E and F; 5 in Fig. 5B; 4 in Fig. 5H–K; 11 in Fig. S4C and D; and one slice closest to the injection site in Fig. 2C and D.

Independent sample *t*-tests, one-way ANOVA followed by the LSD multiple comparison test, a two-sided non-parametric test (Mann-Whitney U-test) and Spearman rank correlation analysis were used to determine statistical differences using SPSS (22.0, International Business Machines Corporation, New York, NY). Statistical significance was set at $^{***}P < 0.001$, $^{**}P < 0.01$ and $^{*}P < 0.05$. All values are presented as the mean ± SEM. Graphs were drawn using Sigma Plot (version 10.0, Systat Software Inc, San Jose, CA).

Results

SAD-RV(ΔG)-N2C(G) Showed a Higher Retrograde Gene Transduction Efficiency but a Similar Labeled Pattern Compared with SAD-RV(ΔG)-B19(G)

First, we packaged SAD-RV(ΔG)-N2C(G)-EGFP and SAD-RV(ΔG)-B19(G)-EGFP (Fig. 1A). To compare their retrograde infection efficiencies *in vivo*, the two pseudotyped viruses were mixed with Alexa Fluor 594

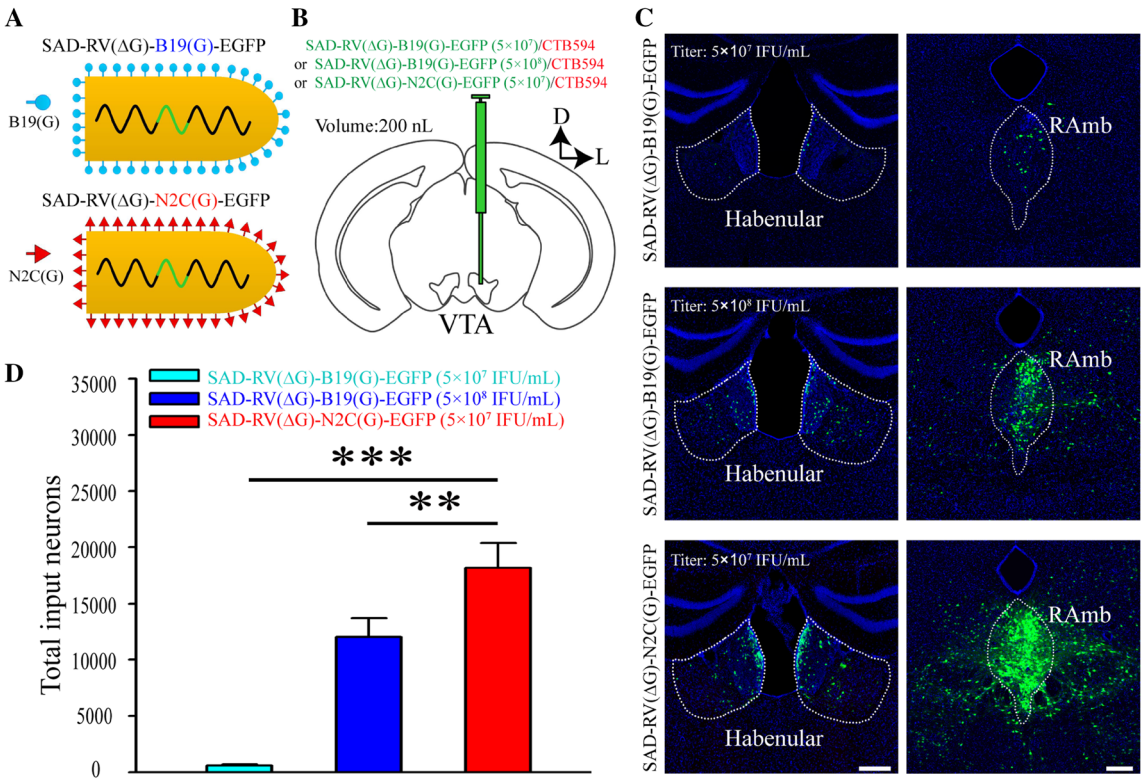

Fig. 1 The retrograde gene transduction efficiency of SAD-RV(ΔG)-N2C(G)-EGFP is higher than that of SAD-RV(ΔG)-B19(G)-EGFP. **A** Schematics of the virion structures of SAD-RV(ΔG)-B19(G)-EGFP (upper panel) and SAD-RV(ΔG)-N2C(G)-EGFP (lower panel). **B** Schematic of the *in vivo* tracing study. A low dose of CTB594 was co-injected with either a low titer of SAD-RV(ΔG)-B19(G)-EGFP (5×10^7 infectious units (IFU)/mL), a high titer of SAD-RV(ΔG)-B19(G)-EGFP (5×10^8 IFU/mL), or SAD-RV(ΔG)-N2C(G)-EGFP (5×10^7 IFU/mL) into the VTA of C57 mice. **C** Many regions upstream of the VTA, such as the habenular nucleus (left panels) and the midbrain raphe nuclei (RAmb, right panels), were retrogradely labeled by SAD-RV(ΔG)-N2C(G)-EGFP (lower panels) or SAD-RV(ΔG)-B19(G)-EGFP with different titers (upper and middle panels). **D** Numbers of neurons in the whole brain retrogradely infected by a low (5×10^7 IFU/mL) or a high (5×10^8 IFU/mL) titer of SAD-RV(ΔG)-B19(G)-EGFP, or SAD-RV(ΔG)-N2C(G)-EGFP (5×10^7 IFU/mL). Scale bars, 200 μm; $n = 4$ mice/group; $^{*}P < 0.05$, $^{**}P < 0.01$, $^{***}P < 0.001$. n.s., no significant difference; one-way ANOVA followed by the LSD multiple comparison test. The nuclei were stained blue by DAPI.

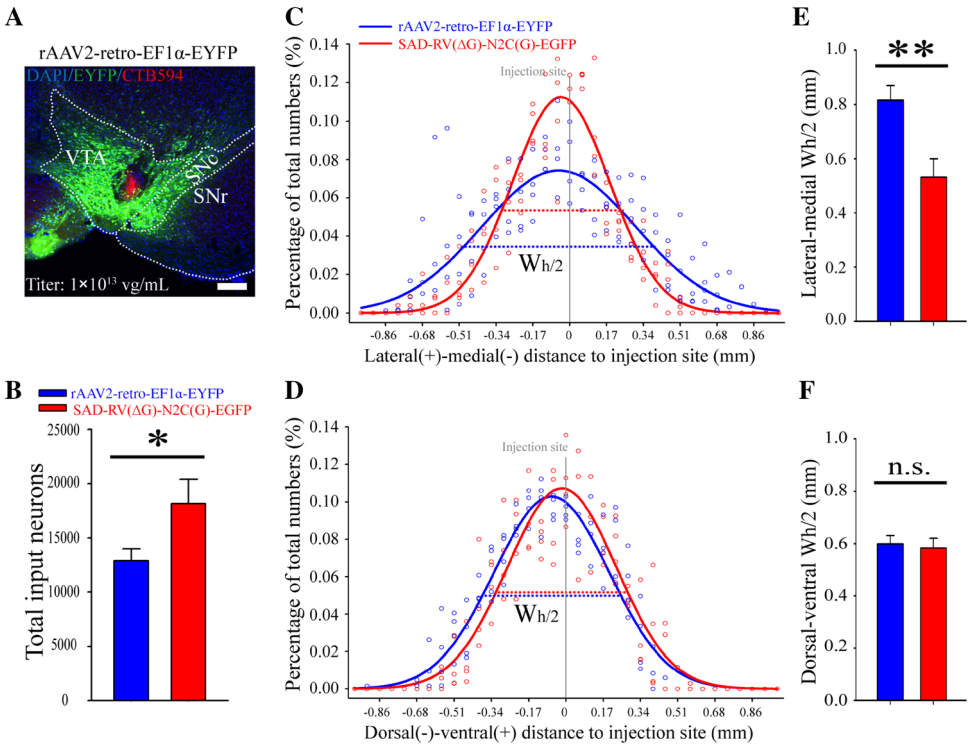

Fig. 2 Retrograde gene transduction efficiency and diffusion range of SAD-RV(ΔG)-N2C(G) and rAAV2-retro. **A** Representative image of the injection site of rAAV2-retro-EF1α-EYFP in the VTA. CTB594 was co-injected to delineate the injection site. SNc: Substantia nigra, compact part; SNr: Substantia nigra, reticular part; VTA: Ventral tegmental area. **B** Numbers of neurons in the whole brain retrogradely infected by SAD-RV(ΔG)-N2C(G)-EGFP (5×10^7 IFU/mL) and rAAV2-retro-EF1α-EYFP (10^{13} IFU/mL). **C**, **D** The lateral-medial (**C**) and dorsal-ventral (**D**) diffusion patterns of rAAV2-retro-EF1α-EYFP (blue dots and line) and SAD-RV(ΔG)-N2C(G)-EGFP (red dots and line) around the injection sites. The signal percentages distributed along the lateral-medial and dorsal-ventral axes of all animals were fitted to Gaussian curves. $W_{h/2}$, peak width at half-height. **E**, **F** Statistical analysis of the lateral-medial (**E**) and dorsal-ventral (**F**) diffusion of rAAV2-retro-EF1α-EYFP and SAD-RV(ΔG)-N2C(G)-EGFP. The $W_{h/2}$ of each animal ($n = 4$ mice/virus) was compared between the two viral groups. $^*P < 0.05$, $^{**}P < 0.01$, $^{***}P < 0.001$. n.s., no significant difference, *t*-test. Scale bar, 200 μm.

conjugated-cholera toxin B subunit (CTB594, red fluorescent signal to mark the injection sites), and injected into the VTA of different mice (Fig. 1B, Table 1). The sections were checked carefully to guarantee that the injection sites were restricted to the VTA (Fig. S1). Otherwise, the samples were excluded. In most of the GFP-labeled regions [midbrain raphe nuclei and the habenular nucleus (Fig. 1C)], SAD-RV(ΔG)-N2C(G)-EGFP clearly infected more neurons than SAD-RV(ΔG)-B19(G)-EGFP, even when the titer of the latter was ten times higher. The whole-brain GFP-positive neuron numbers were also consistent with this result (Fig. 1D, $P = 5.72 \times 10^{-7}$ for viruses at the same titer, $P = 0.0059$ for viruses with tenfold different titers).

The retrograde gene transduction efficiency of the SAD strain RABV was increased by pseudotyping with N2C(G), however, whether the retrograde tropism for neurons in different brain regions was also altered remained unclear. To answer this, GFP-positive neurons within each upstream region were counted and normalized by dividing the total number of retrogradely-labeled neurons in each animal. We found that none of the analyzed regions showed significant differences in input percentage between the SAD-RV(ΔG)-N2C(G)-EGFP and SAD-RV(ΔG)-B19(G)-EGFP groups (Fig. S2A). The percentages of retrogradely-labeled neurons in different regions in the two groups were strongly correlated (Fig. S2B).

These results demonstrated that the RABV with the glycoprotein gene deleted and enveloped with N2C(G) has improved retrograde gene transduction efficiency without affecting the retrograde tropism bias.

SAD-RV(ΔG)-N2C(G) Showed Higher Retrograde Gene Transduction Efficiency and More Restricted Diffusion Range than rAAV2-retro

rAAV2-retro is an outstanding retrograde viral vector mainly due to its high efficiency, and has been broadly used in various functional studies of neuronal circuits [35, 49]. In order to compare the retrograde efficiency of rAAV2-retro

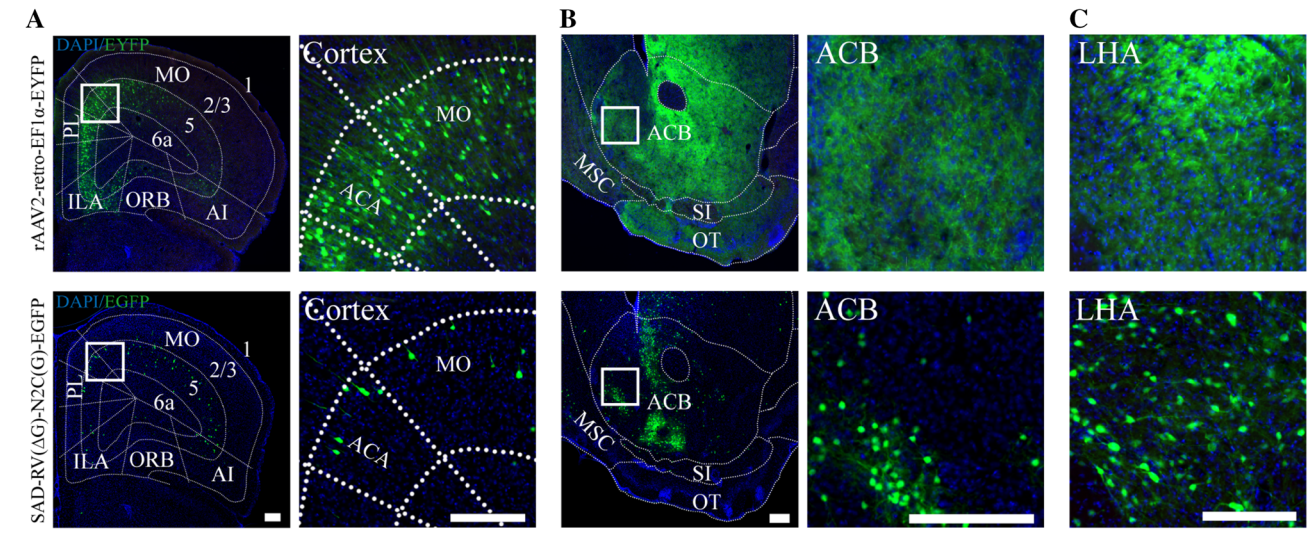
A
B
C
rAAV2-retro-EF1α-EYFP
SAD-RV(ΔG)-N2C(G)-EGFP
DAPI/EYFP
DAPI/EGFP
MO
1
2/3
5
6a
PL
ILA
ORB
AI
Cortex
ACA
ACB
MSC
SI
OT
LHA

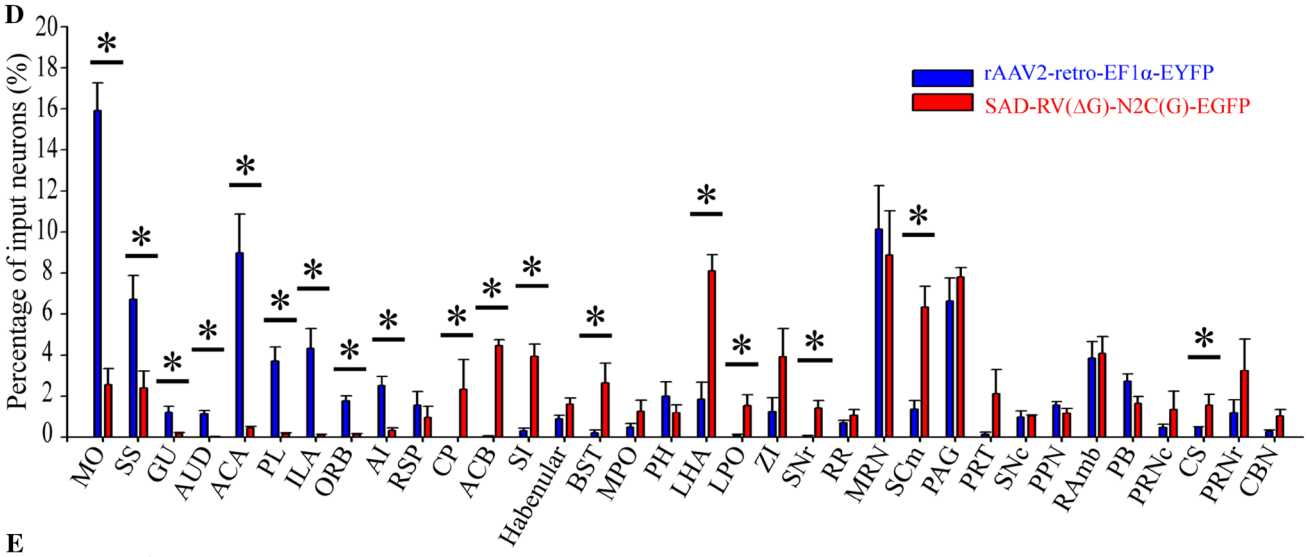
D
Percentage of input neurons (%)
rAAV2-retro-EF1α-EYFP
SAD-RV(ΔG)-N2C(G)-EGFP
MO
SS
GU
AUD
ACA
PL
ILA
ORB
AI
RSP
CP
ACB
SI
Habenular
BST
MPO
PH
LHA
LPO
ZI
SNr
RR
MRN
SCm
PAG
PRT
SNc
PPN
RAmb
PB
PRNc
CS
PRNr
CBN

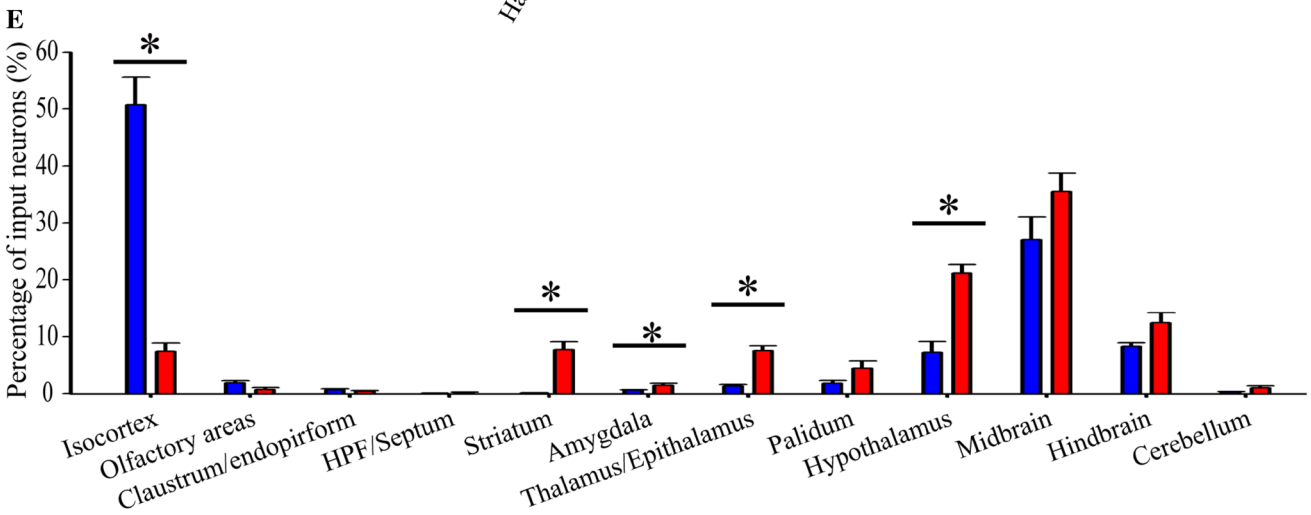
E
Percentage of input neurons (%)
Isocortex
Olfactory areas
Claustrum/endopirform
HPF/Septum
Striatum
Amygdala
Thalamus/Epithalamus
Palidum
Hypothalamus
Midbrain
Hindbrain
Cerebellum

◀**Fig. 3** Retrograde infection tropism biases of SAD-RV(ΔG)-N2C(G) and rAAV2-retro injected into the VTA. **A**-**C** Representative images showing the different retrograde labeling patterns with rAAV2-retro-EF1α-EYFP (upper panels) and SAD-RV(ΔG)-N2C(G)-EGFP (lower panels) in the cortex (**A**), striatum (**B**), and LHA (**C**). **D** Analysis of the input proportions of different nuclei labeled with SAD-RV(ΔG)-N2C(G)-EGFP and rAAV2-retro-EF1α-EYFP. In most nuclei, the input proportions of the neurons labeled with the two viruses were dramatically different. **E** Input proportions of intact brain areas pooled from the discrete nuclei in **D**. Compared with SAD-RV(ΔG)-N2C(G)-EGFP, rAAV2-retro-EF1α-EYFP preferentially infected the isocortex, but rarely infected the striatum, amygdala, pallidum. and hypothalamus. $n = 4$ mice/group; $^{*}P < 0.05$, $^{**}P < 0.01$, $^{***}P < 0.001$. Mann-Whitney U-test. Scale bars, 200 μm. ACB: Nucleus accumbens; ACA: Anterior cingulate area; AI: Agranular insular area; AUD: Auditory areas; BST: Bed nuclei of the stria terminalis; CBN: Cerebellar nuclei; CP: Caudoputamen; CS: Superior central nucleus raphe; GU: Gustatory areas; Habenular: Habenular nucleus; HPF: hippocampal formation; ILA: Infralimbic area; LHA: Lateral hypothalamic area; LPO: Lateral preoptic area; MPO: Medial preoptic area; MO: Somatomotor areas; MRN: Midbrain reticular nucleus; MSC: Medial septal complex; ORB: Orbital area; OT: Olfactory tubercle; PAG: Periaqueductal gray; PB: Parabrachial nucleus; PL: Prelimbic area; PH: Posterior hypothalamic nucleus; PPN: Pedunculopontine nucleus; PRNc: Pontine reticular nucleus, caudal part; PRNr: Pontine reticular nucleus; PRT: Pretectal region; RAmb: Midbrain raphe nuclei; RR: Midbrain reticular nucleus, retrorubral area; RSP: Retrosplenial area; SCm: Superior colliculus, motor related; SI: Substantia innominate; SNc: Substantia nigra, compact part; SNr: Substantia nigra, reticular part; SS: Somatosensory areas; ZI: Zona incerta.

and SAD-RV(ΔG)-N2C(G), rAAV2-retro-EF1α-EYFP was mixed with CTB594 and injected into the VTA (Fig. 2A, Table 1). We found that, compared to the rAAV2-retro-EF1α-EYFP at a titer of 10^{13} viral genomes (vg)/mL, SAD-RV(ΔG)-N2C(G)-EYFP at 5×10^{7} IFU/mL retrogradely infected more neurons (12,891 ± 1,080 for rAAV2-retro-EF1α-EYFP, 18,173 ± 2,232 for SAD-RV(ΔG)-N2C(G)-EGFP), $P = 0.014$; Fig. 2B).

Given that the two viruses were titered using different methods based on their individual properties, and that the number of retrogradely-labeled neurons was positively correlated with the titer, it was difficult to directly compare their retrograde efficiency using different titer units. However, the increased titer could consequently increase the diffusion. Therefore, we further calculated the diffusion patterns of EYFP/GFP+ neuronal somata near the VTA. The rates of virus-labeled neurons were binned every 57.5 μm along the lateral-medial and dorsal-ventral axes and fitted to Gaussian curves. The $W_{h/2}$ was calculated to estimate the diffusion range of the two viruses. We found that, compared with the rAAV2-retro-EF1α-EYFP (10^{13} vg/mL), the $W_{h/2}$ of SAD-RV(ΔG)-N2C(G)-EGFP (5×10^{7} IFU/mL) was much smaller along the lateral-medial axis (Fig. 2C, E), but showed no significant difference along the dorsal-ventral axis (Fig. 2D, F).

Together, these results suggest that SAD-RV(ΔG)-N2C(G)-EGFP has a much higher retrograde gene transduction efficiency and a more limited diffusion range than rAAV2-retro-EF1α-EYFP.

SAD-RV(ΔG)-N2C(G) and rAAV2-retro Exhibited Different Retrograde Infection Tropism in Different Brain Regions

Certain projection neurons have been reported to be refractory to rAAV2-retro infection [35, 40], so we then compared the retrograde infection tropisms of rAAV2-retro and SAD-RV(ΔG)-N2C(G).

To achieve this, we first analyzed the distribution patterns and proportions of EYFP/GFP+ neurons in different brain regions of rAAV2-retro-EF1α-EYFP- and SAD-RV(ΔG)-N2C(G)-EGFP-injected samples. We found that, compared with the SAD-RV(ΔG)-N2C(G)-EGFP, rAAV2-retro-EF1α-EYFP preferentially labeled neurons in the somatomotor, somatosensory, gustatory, auditor, anterior cingulate, prelimbic, infralimbic, orbital, and agranular insular areas (Fig. 3A, D). Whereas, in many of the other regions, such as the caudoputamen (CP), nucleus accumbens (ACB), substantia innominata, bed nuclei of the stria terminalis, lateral hypothalamic area (LHA), lateral preoptic area, substantia nigra, pars reticulata, motor-related superior colliculus, and superior central raphe nucleus, the rAAV2-retro-EF1α-EYFP showed a modest infection efficiency (Fig. 3B–D). It should be noted that, in the CP and ACB, which are greatly enriched with GABAergic neurons and directly connected to the VTA [50–52], very few cell bodies were labeled by rAAV2-retro-EF1α-EYFP. In the periaqueductal gray (PAG), midbrain reticular nucleus, midbrain raphe nuclei and a few other regions, there was no significant difference in the neuronal labeling rate between the two kinds of virus (Fig. 3D).

We further pooled the EYFP/GFP+ neuron signals of every individual brain region into several intact brain areas (Fig. 3E) according to the Allen Brain Atlas (http://www.brain-map.org/). The data showed that in the isocortex, the retrograde neuronal labeling rate of rAAV2-retro-EF1α-EYFP was ~7-fold higher than that of SAD-RV(ΔG)-N2C(G)-EGFP. On the contrary, SAD-RV(ΔG)-N2C(G)-EGFP had a higher percentage of labeled neurons in many non-cortical areas, including the striatum, amygdala, pallidum, and hypothalamus. There was no significant difference in the neuronal labeling rate between the two viruses in the olfactory area, hippocampal formation/septum, claustrum/endopiriform, thalamus/epithalamus, midbrain, hindbrain, and cerebellum (Fig. 3E, Table 2).

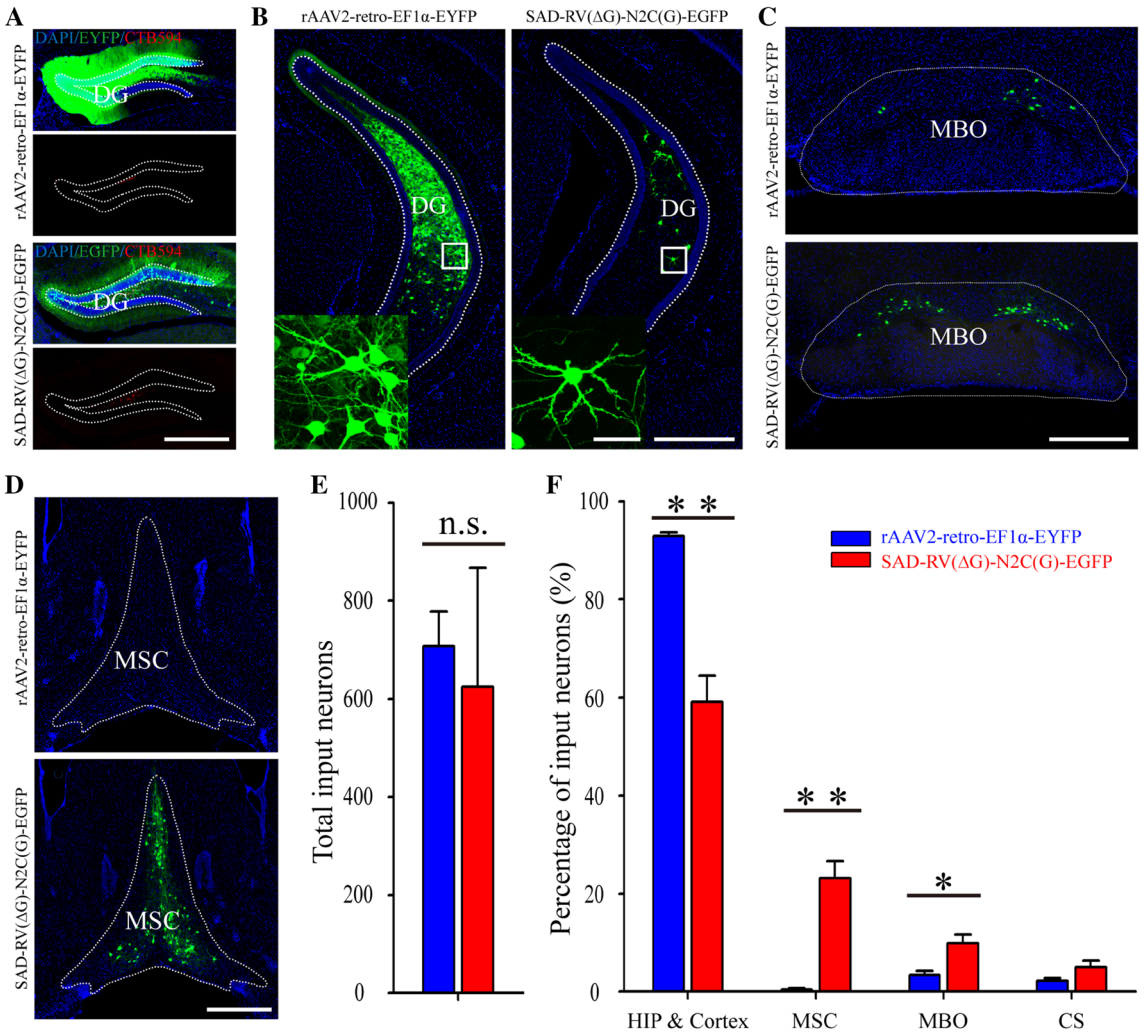

Fig. 4 Different retrograde labeling patterns of SAD-RV(ΔG)-N2C(G)-EGFP and rAAV2-retro-EF1α-EYFP injected into the hippocampus. **A** Coronal sections near the injection sites (indicated by the red signals of CTB594) in the DG by the two viruses (upper panels, rAAV2-retro-EF1α-EYFP; lower panels, SAD-RV(ΔG)-N2C(G)-EGFP). **B**–**D**: Representative images reveal that the retrograde labeling patterns with SAD-RV(ΔG)-N2C(G)-EGFP and rAAV2-retro-EF1α-EYFP are quite different in many regions, such as the hippocampus (**B**), MBO (**C**), and MSC (**D**). **E** Numbers of neurons retrogradely infected with SAD-RV(ΔG)-N2C(G)-EGFP and rAAV2-retro-EF1α-EYFP in the whole brain. **F** Proportions of input from different areas. $n = 3$ mice for rAAV2-retro-EF1α-EYFP; $n = 4$ mice for SAD-RV(ΔG)-N2C(G)-EGFP. $^{*}P < 0.05$, $^{**}P < 0.01$, $^{***}P < 0.001$, *t*-test. Scale bars, 50 μm for insets in **B**, 200 μm for **A**–**D**. CS: Superior central nucleus raphe; DG: Dentate gyrus; HIP: Hippocampal region; MBO: Mammillary body; MSC: Medial septal complex.

To exclude the influence of individual variation and directly compare the retrograde infection tropisms, rAAV2-retro-EF1α-EYFP and SAD-RV(ΔG)-N2C(G)-mCherry were injected separately into the bilateral VTA in the same animal (Fig. S3A and B; Table 1). The differences in the labeling patterns of the two viruses were still observed in these mice (Fig. S3C), consistent with the above results (Fig. 3A–D).

Since the retrograde gene transduction efficiency or tropism biases in different brain regions may differ with the injection site, the two viruses were additionally injected into the dentate gyrus (DG), another region that receives a considerable amount of input from cortical areas (Fig. 4A, Table 1). The images near the injection site showed that the fluorescent signal of rAAV2-retro-EF1α-EYFP was much denser and diffused more widely than SAD-RV(ΔG)-N2C(G)-EGFP (Fig. 4A). Quantitative analysis of the whole-brain GFP/EYFP+ neurons excluding the DG region revealed that SAD-RV(ΔG)-N2C(G)-EGFP at a titer of 5×10^7 IFU/mL had a retrograde gene transduction efficiency comparable to rAAV2-retro-EF1α-EYFP at 10^{13} vg/mL (Fig. 4E, 707 ± 70 for rAAV2-retro-EF1α-EYFP; 625 ± 241 for SAD-RV(ΔG)-N2C(G)-EGFP, $P = 0.40$). We further analyzed the retrogradely-labeled

patterns of the two viruses. Since the hippocampus is a macroscopically defined cortical structure [53, 54], the hippocampus and the cortical areas were collectively referred to as an intact brain area, the hippocampal region (HIP) & Cortex. We found that rAAV2-retro-EF1α-EYFP labeled a greater proportion of projection neurons in the HIP & Cortex (Fig. 4B and F, 92.91% ± 0.74% for rAAV2-retro-EF1α-EYFP; 59.15% ± 5.28% for SAD-RV(ΔG)-N2C(G)-EGFP; $P = 0.0015$) than SAD-RV(ΔG)-N2C(G)-EGFP. However, in the mammillary body (3.39% ± 0.89%, 9.75% ± 1.81%; $P = 0.023$) (Fig. 4C and F) and medial septal complex (MSC, 0.39% ± 0.29%, 23.13% ± 3.54%; $P = 0.0015$) (Fig. 4D and F), the neuronal labeling rate of rAAV2-retro-EF1α-EYFP was ~3- and ~60-folds lower, respectively, despite substantial reports that the DG is densely connected to the MSC [55, 56].

The DG has also been reported to receive abundant contralateral hippocampal inputs [57, 58]. To investigate the retrograde infection tropism in more detail, we further compared the labeling patterns of the two viruses in the contralateral hippocampus. The proportion of EYFP/GFP+ neurons in each contralateral subregion was normalized to all contralateral hippocampal inputs. We found that the retrograde labeling patterns in the contralateral subregions were significantly different. The rAAV2-retro-EF1α-EYFP-labeled neurons were highly enriched in the contralateral DG (99.35% ± 0.41% for rAAV2-retro-EF1α-EYFP and 27.02% ± 6.81% for SAD-RV(ΔG)-N2C(G)-EGFP; $P = 0.00014$), especially in the dorsal DG (Fig. S4A and C), but only sparsely distributed in CA3, CA2, and CA1. However, neurons labeled with SAD-RV(ΔG)-N2C(G)-EGFP were mainly found in the contralateral CA3 (0.33% ± 0.20% for rAAV2-retro-EF1α-EYFP and 60.51% ± 5.83% for SAD-RV(ΔG)-N2C(G)-EGFP; $P = 0.00016$), while also scattered throughout the DG, CA2, and CA1 (Fig. S4A and C). Since the contralateral DG neurons labeled with rAAV2-retro-EF1α-EYFP were predominant in the posterior ventral rather than the anterior dorsal part, we then analyzed the rostral-caudal distribution of the contralateral hippocampal EYFP/GFP+ neurons. We found that the rAAV2-retro-EF1α-EYFP mainly infected the caudal but not the rostral hippocampus. On the contrary, the SAD-RV(ΔG)-N2C(G)-EGFP mainly targeted neurons in the rostral hippocampus, which was close to the injection site, while also slightly labeled every part of the contralateral hippocampus along the rostral-caudal axis (Fig. S4B and D).

We also established that after the virus was injected into the VTA or the DG, neurons in several regions (ACB for the VTA and MSC, and contralateral CA1, CA2 and CA3 for the DG) were resistant to retrograde infection with rAAV2-retro-EF1α-EYFP, while the SAD-RV(ΔG)-N2C(G)-EGFP was able to infect all of these regions. These results suggest that the retrograde infection biases in rAAV2-retro-EF1α-EYFP and SAD-RV(ΔG)-N2C(G)-EGFP are quite different. The rAAV2-retro-EF1α-EYFP prefers to infect cortical more than subcortical neurons, while SAD-RV(ΔG)-N2C(G)-EGFP showed a less biased retrograde infection tropism for neurons in different regions.

SAD-RV(ΔG)-N2C(G) and rAAV2-retro Exhibited Different Efficiencies in Retrogradely Labeling Long-Projection Inhibitory Neurons

rAAV2-retro-EF1α-EYFP exhibited highly biased labeling patterns among different regions; that is, there was a strong preference for retrograde labeling in the long-projection cortical and hippocampal neurons, which mainly consist of excitatory subtypes [59–61], and a markedly lower tendency to label regions where GABAergic neurons are dominant. Therefore, we speculated as to whether the different retrograde infection patterns of rAAV2-retro-EF1α-EYFP and SAD-RV(ΔG)-N2C(G)-EGFP were due to their tropisms toward different neuronal subtypes. To test this hypothesis, VTA-injected cortical samples were selected and immnohistochemically stained for Ca^{2+}/-calmodulin-dependent protein kinase II (CaMKII), a marker for excitatory neurons in the cortex [62, 63] (Fig. 5A). The results showed that the neurons retrogradely labeled by both rAAV2-retro-EF1α-EYFP and SAD-RV(ΔG)-N2C(G)-EGFP were highly co-labeled with CaMKII, showing no significant difference, although the rAAV2-retro-EF1α-EYFP group exhibited a slightly tendency to higher co-labeling (Fig. 5B). Thus, we further investigated the retrograde infection properties of the two viruses for long-projection inhibitory neurons.

To achieve this, rAAV2-retro-EF1α-mCherry and SAD-RV(ΔG)-N2C(G)-mCherry were separately injected into the VTA of GAD67-GFP mice (Table 1). We found that neither of the viruses labeled inhibitory neurons in the cortex (Fig. 5C). In the ACB, which was refractory to infection, rAAV2-retro showed that about half of the SAD-RV(ΔG)-N2C(G)-mCherry-labeled neurons were inhibitory (Fig. 5D and H). In the zona incerta, LHA, and PAG, SAD-RV(ΔG)-N2C(G)-mCherry labeled a significantly higher proportion of GAD67-GFP neurons than rAAV2-retro-EF1α-EYFP (Fig. 5E–G, and I–K).

These results indicate that rAAV2-retro is less efficient in retrogradely infecting long-projection inhibitory neurons than SAD-RV(ΔG)-N2C(G), which may contribute to the different retrograde infection patterns of the two viruses.

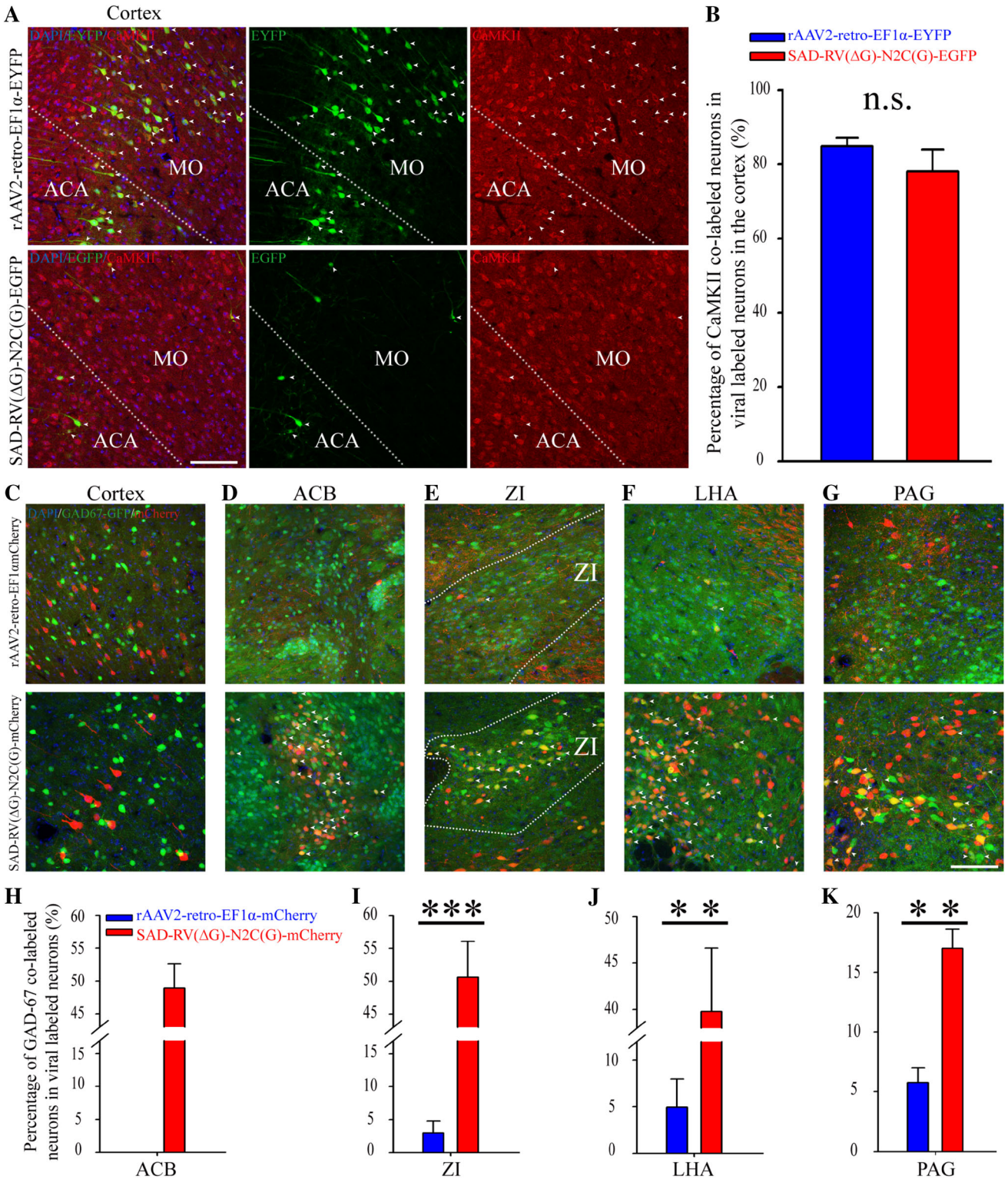
A
Cortex
DAPI/EYFP/CaMKII
EYFP
CaMKII
rAAV2-retro-EF1α-EYFP
MO
ACA
DAPI/EGFP/CaMKII
EGFP
SAD-RV(ΔG)-N2C(G)-EGFP
B
rAAV2-retro-EF1α-EYFP
SAD-RV(ΔG)-N2C(G)-EGFP
n.s.
Percentage of CaMKII co-labeled neurons in viral labeled neurons in the cortex (%)
C
Cortex
DAPI/GAD67-GFP/mCherry
rAAV2-retro-EF1αmCherry
SAD-RV(ΔG)-N2C(G)-mCherry
D
ACB
E
ZI
F
LHA
G
PAG
H
rAAV2-retro-EF1α-mCherry
SAD-RV(ΔG)-N2C(G)-mCherry
Percentage of GAD-67 co-labeled neurons in viral labeled neurons (%)
ACB
I
***
ZI
J
**
LHA
K
**
PAG

◀**Fig. 5** rAAV2-retro and SAD-RV(ΔG)-N2C(G) exhibited different efficiencies in retrograde labeling of long-projection inhibitory neurons. **A** Representative cortical images displaying the co-localization (merged, left) of virus-labeled neurons (green, middle), and immunofluorescent CaMKII staining (red, right). **B** The CaMKII-positive rates of EYFP/GFP+ labeled neurons with SAD-RV(ΔG)-N2C(G)-EGFP and rAAV2-retro-EF1α-EYFP in cortical regions. n.s., no significant difference, Mann-Whitney U-test. **C–G** Representative images showing the co-localization of GAD67-GFP (green, GAD 67-GFP mice) and neurons labeled with rAAV2-retro-EF1α-mCherry (red, upper panels) and SAD-RV(ΔG)-N2C(G)-mCherry (red, lower panels) in cortex (**C**), ACB (**D**), ZI (**E**), LHA (**F**), and PAG (**G**). **H–K** Analysis of co-labeling rates of GAD67-GFP with virus-labeled (red) neurons. SAD-RV(ΔG)-N2C(G)-mCherry labeled more GAD67-GFP-positive neurons than rAAV2-retro-EF1α-mCherry in the ACB (**H**), ZI (**I**), LHA (**J**), and PAG (**K**). $n = 3$ mice for rAAV2-retro-EF1α-mCherry; $n = 4$ mice for SAD-RV(ΔG)-N2C(G)-mCherry. $^{*}P < 0.05$, $^{**}P < 0.01$, $^{***}P < 0.001$, *t*-test; scale bars, 200 μm. ACA: Anterior cingulate area; ACB: Nucleus accumbens; MO: Somatomotor areas; LHA: Lateral hypothalamic area; ZI: Zona incerta; PAG: Periaqueductal gray.

Discussion

RABV has been widely used to target long-projecting neuronal networks by either the trans-monosynaptic spread or direct retrograde infection at the terminals. When used as a retrograde tracer, RABV is largely limited by its low efficiency. Here, we found that the N2C glycoprotein derived from the RABV CVS strain was able to increase the *in vivo* retrograde gene transduction efficiency of the SAD strain more than tenfold. Furthermore, the pseudotyped virus SAD-RV(ΔG)-N2C(G) showed a comparable retrograde efficiency, but a more localized diffusion range and a broader tropism to different types and regions of long-projecting neuronal populations than rAAV2-retro.

SAD-RV(ΔG)-N2C(G) is Highly Efficient for Retrograde Tracing

It has been reported that CVS-RV(ΔG)-N2C(G) possesses higher neuronal invasiveness [64] and greater retrograde trans-synaptic spread [46] than the vaccine strain SAD-RV(ΔG)-B19(G). When pseudotyped with N2C(G), SAD-RV(ΔG)-N2C(G) also exhibits greater neuro-tropism in cell culture than SAD-RV(ΔG)-B19(G) [45]. However, a recent study [65] found that complementing SAD-RV(ΔG) with N2C(G) showed less or similar retrograde trans-synaptic efficiency than with B19(G). Besides, the mechanisms of retrograde trans-synaptic spread and retrograde infection at axon terminals could be different. Thus, comparison of the retrograde gene transduction efficiency between SAD-RV(ΔG)-B19(G) and SAD-RV(ΔG)-N2C(G) still remained obscure. We addressed this conundrum in the present work and found that, after injecting virus into the VTA, the *in vivo* retrograde gene transduction efficiency of SAD-RV(ΔG)-N2C(G) was much higher than that of SAD-RV(ΔG)-B19(G) (Fig. 1D). Our results are consistent with findings reported in earlier studies. Other than the enhanced neuronal invasiveness, the retrograde labeling patterns in SAD-RV(ΔG)-N2C(G) and SAD-RV(ΔG)-B19(G) were not significantly different (Fig. S2). A possible explanation for the similar labeling patterns is that N2C(G) might infect long-projecting neurons *via* the same receptors but with a much higher affinity than B19(G).

rAAV2-retro is also an outstanding viral tool to efficiently target long-projecting neurons. In this study, we found that the retrograde gene transduction efficiency of SAD-RV(ΔG)-N2C(G) was no less than that of rAAV2-retro (Fig. 2B and 4E), but had a more restricted diffusion

Table 1 Experimental parameters for retrograde tracing.

Animal	Number	Nucleus	Virus	Dose (IFU/mL or viral genomes/mL)	Volume (μL)	Injection (Day)	Perfusion (Day)
C57BL/6	4	VTA	SAD-RV(ΔG)-B19(G)-EGFP	5×10^7	0.2	Day1	Day7
C57BL/6	4	VTA	SAD-RV(ΔG)-B19(G)-EGFP	5×10^8	0.2	Day1	Day7
C57BL/6	4	VTA	SAD-RV(ΔG)-N2C(G)-EGFP	5×10^7	0.2	Day1	Day7
C57BL/6	4	VTA	rAAV2-retro-Ef1α-EYFP	1×10^{13}	0.2	Day1	Day21
C57BL/6	4	VTA(Right)	rAAV2-retro-Ef1α-EYFP	1×10^{13}	0.2	Day1	Day21
		VTA(Left)	SAD-RV(ΔG)-N2C(G)-mCherry	1.1×10^8	0.2	Day14	
C57BL/6	4	DG	SAD-RV(ΔG)-N2C(G)-EGFP	5×10^7	0.1	Day1	Day7
C57BL/6	3	DG	rAAV2-retro-Ef1α-EYFP	1×10^{13}	0.1	Day1	Day21
GAD67-GFP	4	VTA	SAD-RV(ΔG)-N2C(G)-mCherry	1.1×10^8	0.2	Day1	Day7
GAD67-GFP	3	VTA	rAAV2-retro-Ef1α-mCherry	1.68×10^{13}	0.2	Day1	Day21

Table 2 Retrograde neuronal labeling rate in brain regions.

Brain regions	Values (Mean ± SEM)		*P*
	rAAV2-retro-EF1α-EYFP	SAD-RV(ΔG)-N2C(G)-EGFP	
Isocortex	50.72% ± 4.85%	7.42% ± 1.47%	0.029
Striatum	0.08% ± 0.05%	7.76% ± 1.37%	0.029
Amygdala	0.62% ± 0.05%	1.44% ± 0.38%	0.029
Pallidum	1.30% ± 0.27%	7.57% ± 0.86%	0.029
Hypothalamus	7.27% ± 1.87%	21.14% ± 1.56%	0.029
Olfactory area	1.90% ± 0.33%	0.69% ± 0.38%	0.057
Hippocampal formation (HPF)/septum	0.64% ± 0.19%	0.37% ± 0.16%	0.34
Claustrum/endopiriform	0.04% ± 0.05%	0.20% ± 0.07%	0.11
Thalamus/epithalamus	1.81% ± 0.48%	4.44% ± 1.25%	0.11
Midbrain	27.00% ± 4.07%	35.50% ± 3.26%	0.20
Hindbrain	8.34% ± 0.59%	12.43% ± 1.79%	0.057
Cerebellum	0.28% ± 0.08%	1.03% ± 0.34%	0.057

range (Fig 2C, E and 4A). This may be due to the different virion sizes [6, 26, 66, 67]. Although the number of retrogradely-labeled neurons further increased with the titer of rAAV2-retro, this could lead to a larger range of viral diffusion, which subsequently raises the risk of non-specific infection of neurons upstream from the regions adjacent to the injection site. With retrograde efficiency comparable to rAAV2-retro, the more localized diffusion range of SAD-RV(ΔG)-N2C(G) could make it more suitable to target the neuronal inputs to small nuclei.

The recently-developed receptor complementation strategy for CAV-2 has also extensively improved its retrograde transport efficiency and overcome the limitation of biased tropism [34]. However, this strategy needs an additional viral injection prior to the CAV-2-Cre, which complicates animal surgery, and makes it hard to access difficult-to-inject areas or target a large volume or even whole-brain upstream tissues. SAD-RV(ΔG)-N2C(G), with its intrinsic high efficiency and broad tropism, should be able to overcome these limitations. However, further studies analyzing the efficiency of CAV-2 and SAD-RV(ΔG)-N2C(G) in different neuronal circuits will also be valuable in guiding the applications of these viral tools.

The Retrograde Neuronal Tropism Biases of rAAV2-retro and SAD-RV(ΔG)-N2C(G) are Different

In the present study, we showed that AAV2-retro and SAD-RV(ΔG)-N2C(G), when injected either into the VTA or DG, displayed different retrograde labeling patterns. Some regions, especially the striatum and basal forebrain, were largely resistant to retrograde infection by rAAV2-retro, but susceptible to SAD-RV(ΔG)-N2C(G) (Fig. 3B and 4D), showing that SAD-RV(ΔG)-N2C(G) has a broader retrograde tropism for long-projecting neurons.

Our experimental data on the selectivity of SAD-RV(ΔG)-N2C(G) and rAAV2-retro for the two most dominant neuron types, CaMKII+ and GAD67+, showed that few neurons labeled with rAAV2-retro were long-projecting GABAergic, while a significant percentage of the SAD-RV(ΔG)-N2C(G)-labeled neurons (from 17 to 50 in subcortical regions) were long-projecting GABAergic neurons (Fig. 5D–K). However, it should be noted that most of the long-projecting neurons in the cortex are excitatory [59, 60, 68] (Fig. 5A, B). Therefore, the distinct retrograde infection preference of the two viruses over excitatory and inhibitory long-projection neurons generated different input patterns for a given region. The VTA receives extensive subcortical neuronal innervation [69, 70], while the major inputs to the DG are from cortical and hippocampal subregions [57, 58]. In the present study, we found that rAAV2-retro with the EF1α promoter was much more efficient in labeling long-projecting cortical and hippocampal excitatory neurons. This is partially consistent with previous reports that compared the properties of SAD-RV(ΔG)-B19(G) and rAAV2-retro with the CMV promoter [44]. However, we still cannot exclude the possibility that the observed differences in retrograde tropism between RABV (viral endogenous promoter) and rAAV2-retro (EF1α promoter) could be affected by the different promoters used here.

Indeed, the input patterns of the VTA and the DG revealed by the two viruses are rather different (Fig. 3D, E,4F, S4C, D). The significantly different neuronal tropisms shown by these results suggest that when tracing

data are interpreted, the viral tools should be considered carefully. In fact, RABV may also exhibit tropism biases in some cases [71]. Thus, the best selection of viral tools depends on the specific circuit being studied, and the combined use of multiple viral tracers should get us closer to the actual facts.

Although we demonstrated that SAD-RV(ΔG)-N2C(G) has high efficiency and broad tropism for retrograde labeling of neuronal circuits, further work is still required to overcome the viral cytotoxicity for achieving long-term functional studies or transgenic expression. Fortunately, recently-developed strategies which delete certain genes [40] or introduce a self-inactivating vector [44] of SAD-RV(ΔG) have successfully overcome this limitation. One might argue that CVS-RV(ΔG)-N2C(G) is less toxic than SAD-RV(ΔG)-N2C(G) and hence is superior. However, since the virus production is much easier for SAD-RV(ΔG) than for CVS-RV(ΔG), and the most potent designs [40, 44] to reduce the toxicity of RABV to date are based on the SAD-RV(ΔG) vector, our introduction of SAD-RV(ΔG)-N2C(G) and our ongoing research to integrate these systems could provide more easily accessible and promising retrograde tools for the community.

In summary, we have provided experimental evidence for a powerful viral tool, N2C(G)-enveloped SAD-RV(ΔG)-N2C(G), which has high retrograde gene transduction efficiency and broad neuro-tropism to target the inputs to neuronal circuits. The comparison of the infection efficiency and neuro-tropism of SAD-RV(ΔG)-N2C(G) and rAAV2-retro provides valuable information for the selection of these viruses for individual research designs.

Acknowledgements We thank Yue Liu and Aolin Cai from Wuhan Institute of Physics and Mathematics for help with data analysis; Yanqiu Li, Yuanli Liao, and Pingping An from Wuhan Institute of Physics and Mathematics for maintaining and genotyping the GAD 67-GFP mice, and Lingling Xu from Wuhan Institute of Physics and Mathematics for capturing confocal images. This work was supported by the National Basic Research Program (973 Program) of China (2015CB755601), the Strategic Priority Research Program of the Chinese Academy of Sciences (XDB32030200), the National Natural Science Foundation of China (31771156, 81661148053, 91632303, 31800885, 31500868, 31671120 and 91732304), and the China Postdoctoral Science Foundation (2019M653118 and 2018M632946).

Conflict of interest The authors declare that they have no competing interests.

References

1. Abeles M. Corticonics: Neural Circuits of the Cerebral Cortex. Cambridge University Press, 1991.
2. Tomioka R, Okamoto K, Furuta T, Fujiyama F, Iwasato T, Yanagawa Y, *et al.* Demonstration of long-range GABAergic connections distributed throughout the mouse neocortex. Eur J Neurosci 2005, 21: 1587–1600.
3. Gayoso J, Castro A, Anadon R, Manso MJ. Crypt cells of the zebrafish Danio rerio mainly project to the dorsomedial glomerular field of the olfactory bulb. Chem Senses 2012, 37: 357–369.
4. Huang ZJ. Toward a genetic dissection of cortical circuits in the mouse. Neuron 2014, 83: 1284–1302.
5. Miller MW, Vogt BA. Direct connections of rat visual cortex with sensory, motor, and association cortices. J Comp Neurol 1984, 226: 184–202.
6. Osakada F, Callaway EM. Design and generation of recombinant rabies virus vectors. Nat Protoc 2013, 8: 1583–1601.
7. Su YT, Gu MY, Chu X, Feng X, Yu YQ. Whole-brain mapping of direct inputs to and axonal projections from GABAergic neurons in the parafacial zone. Neurosci Bull 2018, 34: 485–496.
8. Roselli F, Caroni P. A circuit mechanism for neurodegeneration. Cell 2012, 151: 250–252.
9. Rubinov M, Bullmore E. Fledgling pathoconnectomics of psychiatric disorders. Trends Cogn Sci 2013, 17: 641–647.
10. Zhai S, Tanimura A, Graves SM, Shen W, Surmeier DJ. Striatal synapses, circuits, and Parkinson's disease. Curr Opin Neurobiol 2017, 48: 9–16.
11. Fullard ME, Morley JF, Duda JE. Olfactory dysfunction as an early biomarker in Parkinson's disease. Neurosci Bull 2017, 33: 515–525.
12. Gratwicke J, Jahanshahi M, Foltynie T. Parkinson's disease dementia: a neural networks perspective. Brain 2015, 138: 1454–1476.
13. Taverna S, Ilijic E, Surmeier DJ. Recurrent collateral connections of striatal medium spiny neurons are disrupted in models of Parkinson's disease. J Neurosci 2008, 28: 5504–5512.
14. Verret L, Mann EO, Hang GB, Barth AM, Cobos I, Ho K, *et al.* Inhibitory interneuron deficit links altered network activity and cognitive dysfunction in Alzheimer model. Cell 2012, 149: 708–721.
15. Milnerwood AJ, Raymond LA. Early synaptic pathophysiology in neurodegeneration: insights from Huntington's disease. Trends Neurosci 2010, 33: 513–523.
16. Vercelli A, Repici M, Garbossa D, Grimaldi A. Recent techniques for tracing pathways in the central nervous system of developing and adult mammals. Brain Res Bull 2000, 51: 11–28.
17. Katz LC. Local circuitry of identified projection neurons in cat visual cortex brain slices. J Neurosci 1987, 7: 1223–1249.
18. Stoeckel K, Schwab M, Thoenen H. Role of gangliosides in the uptake and retrograde axonal transport of cholera and tetanus toxin as compared to nerve growth factor and wheat germ agglutinin. Brain Res 1977, 132: 273–285.
19. Conte WL, Kamishina H, Reep RL. Multiple neuroanatomical tract-tracing using fluorescent Alexa Fluor conjugates of cholera toxin subunit B in rats. Nat Protoc 2009, 4: 1157–1166.
20. Katz L, Burkhalter A, Dreyer W. Fluorescent latex microspheres as a retrograde neuronal marker for *in vivo* and *in vitro* studies of visual cortex. Nature 1984, 310: 498.
21. Ni RJ, Luo PH, Shu YM, Chen JT, Zhou JN. Whole-brain mapping of afferent projections to the bed nucleus of the stria terminalis in tree shrews. Neuroscience 2016, 333: 162–180.
22. Gabriele ML, Smoot JE, Jiang H, Stein BE, McHaffie JG. Early establishment of adult-like nigrotectal architecture in the neonatal cat: a double-labeling study using carbocyanine dyes. Neuroscience 2006, 137: 1309–1319.
23. Ugolini G. Rabies virus as a transneuronal tracer of neuronal connections. Adv Virus Res 2011, 79: 165–202.
24. Callaway EM, Luo L. Monosynaptic circuit tracing with glycoprotein-deleted rabies viruses. J Neurosci 2015, 35: 8979–8985.
25. Wickersham IR, Finke S, Conzelmann KK, Callaway EM. Retrograde neuronal tracing with a deletion-mutant rabies virus. Nat Methods 2007, 4: 47–49.

26. Kelly RM, Strick PL. Rabies as a transneuronal tracer of circuits in the central nervous system. J Neurosci Methods 2000, 103: 63–71.
27. Ugolini G, Kuypers H, Simmons A. Retrograde transneuronal transfer of herpes simplex virus type 1 (HSV 1) from motoneurones. Brain Res 1987, 422: 242–256.
28. Xu C, Krabbe S, Grundemann J, Botta P, Fadok JP, Osakada F, *et al.* Distinct hippocampal pathways mediate dissociable roles of context in memory retrieval. Cell 2016, 167: 961–972 e916.
29. Cuchet D, Potel C, Thomas J, Epstein AL. HSV-1 amplicon vectors: a promising and versatile tool for gene delivery. Expert Opin Biol Ther 2007, 7: 975–995.
30. Lilley CE, Groutsi F, Han Z, Palmer JA, Anderson PN, Latchman DS, *et al.* Multiple immediate-early gene-deficient herpes simplex virus vectors allowing efficient gene delivery to neurons in culture and widespread gene delivery to the central nervous system *in vivo*. J Virol 2001, 75: 4343–4356.
31. Frampton AR, Jr., Goins WF, Nakano K, Burton EA, Glorioso JC. HSV trafficking and development of gene therapy vectors with applications in the nervous system. Gene Ther 2005, 12: 891–901.
32. Soudais C, Laplace-Builhe C, Kissa K, Kremer EJ. Preferential transduction of neurons by canine adenovirus vectors and their efficient retrograde transport *in vivo*. FASEB J 2001, 15: 2283–2285.
33. Junyent F, Kremer EJ. CAV-2–why a canine virus is a neurobiologist's best friend. Curr Opin Pharmacol 2015, 24: 86–93.
34. Li SJ, Vaughan A, Sturgill JF, Kepecs A. A viral receptor complementation strategy to overcome CAV-2 tropism for efficient retrograde targeting of neurons. Neuron 2018, 98: 905–917 e905.
35. Tervo DG, Hwang BY, Viswanathan S, Gaj T, Lavzin M, Ritola KD, *et al.* A designer AAV variant permits efficient retrograde access to projection neurons. Neuron 2016, 92: 372–382.
36. Cronin J, Zhang XY, Reiser J. Altering the tropism of lentiviral vectors through pseudotyping. Curr Gene Ther 2005, 5: 387–398.
37. Kato S, Kobayashi K, Inoue K, Kuramochi M, Okada T, Yaginuma H, *et al.* A lentiviral strategy for highly efficient retrograde gene transfer by pseudotyping with fusion envelope glycoprotein. Hum Gene Ther 2011, 22: 197–206.
38. Hirano M, Kato S, Kobayashi K, Okada T, Yaginuma H, Kobayashi K. Highly efficient retrograde gene transfer into motor neurons by a lentiviral vector pseudotyped with fusion glycoprotein. PLoS One 2013, 8: e75896.
39. Coulon P, Derbin C, Kucera P, Lafay F, Prehaud C, Flamand A. Invasion of the peripheral nervous systems of adult mice by the CVS strain of rabies virus and its avirulent derivative AvO1. J Virol 1989, 63: 3550–3554.
40. Chatterjee S, Sullivan HA, MacLennan BJ, Xu R, Hou Y, Lavin TK, *et al.* Nontoxic, double-deletion-mutant rabies viral vectors for retrograde targeting of projection neurons. Nat Neurosci 2018, 21: 638–646.
41. Senn V, Wolff SB, Herry C, Grenier F, Ehrlich I, Grundemann J, *et al.* Long-range connectivity defines behavioral specificity of amygdala neurons. Neuron 2014, 81: 428–437.
42. Follenzi A, Santambrogio L, Annoni A. Immune responses to lentiviral vectors. Curr Gene Ther 2007, 7: 306–315.
43. Themis M, Waddington SN, Schmidt M, Von Kalle C, Wang Y, Al-Allaf F, *et al.* Oncogenesis following delivery of a nonprimate lentiviral gene therapy vector to fetal and neonatal mice. Mol Ther 2005, 12: 763–771.
44. Ciabatti E, Gonzalez-Rueda A, Mariotti L, Morgese F, Tripodi M. Life-long genetic and functional access to neural circuits using self-inactivating rabies virus. Cell 2017, 170: 382–392 e314.
45. Hagendorf N, Conzelmann KK. Pseudotyping of G-gene-deficient rabies virus. Cold Spring Harb Protoc 2015, 2015: pdb prot089417.
46. Reardon TR, Murray AJ, Turi GF, Wirblich C, Croce KR, Schnell MJ, *et al.* Rabies virus CVS-N2c(DeltaG) strain enhances retrograde synaptic transfer and neuronal viability. Neuron 2016, 89: 711–724.
47. Tamamaki N, Yanagawa Y, Tomioka R, Miyazaki J, Obata K, Kaneko T. Green fluorescent protein expression and colocalization with calretinin, parvalbumin, and somatostatin in the GAD67-GFP knock-in mouse. J Comp Neurol 2003, 467: 60–79.
48. Osakada F, Mori T, Cetin AH, Marshel JH, Virgen B, Callaway EM. New rabies virus variants for monitoring and manipulating activity and gene expression in defined neural circuits. Neuron 2011, 71: 617–631.
49. Capelli P, Pivetta C, Soledad Esposito M, Arber S. Locomotor speed control circuits in the caudal brainstem. Nature 2017, 551: 373–377.
50. Yang H, de Jong JW, Tak Y, Peck J, Bateup HS, Lammel S. Nucleus accumbens subnuclei regulate motivated behavior *via* direct inhibition and disinhibition of VTA dopamine subpopulations. Neuron 2018, 97: 434–449 e434.
51. Watabe-Uchida M, Zhu L, Ogawa SK, Vamanrao A, Uchida N. Whole-brain mapping of direct inputs to midbrain dopamine neurons. Neuron 2012, 74: 858–873.
52. Ogawa SK, Cohen JY, Hwang D, Uchida N, Watabe-Uchida M. Organization of monosynaptic inputs to the serotonin and dopamine neuromodulatory systems. Cell Rep 2014, 8: 1105–1118.
53. Watson C, Paxinos G, Puelles L. The mouse nervous system. Academic Press, 2012.
54. Isaacson R. The Hippocampus: Volume 1: Structure and Development. Springer Science & Business Media, 2012.
55. Vivar C, Potter MC, Choi J, Lee JY, Stringer TP, Callaway EM, *et al.* Monosynaptic inputs to new neurons in the dentate gyrus. Nat Commun 2012, 3: 1107.
56. Semba K. Multiple output pathways of the basal forebrain: organization, chemical heterogeneity, and roles in vigilance. Behav Brain Res 2000, 115: 117–141.
57. Sun Y, Grieco SF, Holmes TC, Xu X. Local and long-range circuit connections to hilar mossy cells in the dentate gyrus. eNeuro 2017, 4.
58. Bui AD, Nguyen TM, Limouse C, Kim HK, Szabo GG, Felong S, *et al.* Dentate gyrus mossy cells control spontaneous convulsive seizures and spatial memory. Science 2018, 359: 787–790.
59. Molyneaux BJ, Arlotta P, Menezes JR, Macklis JD. Neuronal subtype specification in the cerebral cortex. Nat Rev Neurosci 2007, 8: 427.
60. Lodato S, Rouaux C, Quast KB, Jantrachotechatchawan C, Studer M, Hensch TK, *et al.* Excitatory projection neuron subtypes control the distribution of local inhibitory interneurons in the cerebral cortex. Neuron 2011, 69: 763–779.
61. Bezaire MJ, Soltesz I. Quantitative assessment of CA1 local circuits: knowledge base for interneuron-pyramidal cell connectivity. Hippocampus 2013, 23: 751–785.
62. Hayashi Y, Shi SH, Esteban JA, Piccini A, Poncer JC, Malinow R. Driving AMPA receptors into synapses by LTP and CaMKII: requirement for GluR1 and PDZ domain interaction. Science 2000, 287: 2262–2267.
63. Miller SG, Kennedy MB. Distinct forebrain and cerebellar isozymes of type II Ca2+/calmodulin-dependent protein kinase associate differently with the postsynaptic density fraction. J Biol Chem 1985, 260: 9039–9046.
64. Morimoto K, Hooper DC, Carbaugh H, Fu ZF, Koprowski H, Dietzschold B. Rabies virus quasispecies: implications for pathogenesis. Proc Natl Acad Sci U S A 1998, 95: 3152–3156.

65. Kim EJ, Jacobs MW, Ito-Cole T, Callaway EM. Improved monosynaptic neural circuit tracing using engineered rabies virus glycoproteins. Cell Rep 2016, 15: 692–699.
66. Daya S, Berns KI. Gene therapy using adeno-associated virus vectors. Clin Microbiol Rev 2008, 21: 583–593.
67. Ayuso E, Mingozzi F, Bosch F. Production, purification and characterization of adeno-associated vectors. Curr Gene Ther 2010, 10: 423–436.
68. Bezaire MJ, Soltesz I. Quantitative assessment of CA1 local circuits: knowledge base for interneuron-pyramidal cell connectivity. Hippocampus 2013, 23: 751–785.
69. Beier KT, Steinberg EE, DeLoach KE, Xie S, Miyamichi K, Schwarz L, *et al.* Circuit architecture of VTA dopamine neurons revealed by systematic input-output mapping. Cell 2015, 162: 622–634.
70. Ogawa SK, Watabe-Uchida M. Organization of dopamine and serotonin system: Anatomical and functional mapping of monosynaptic inputs using rabies virus. Pharmacol Biochem Behav 2018, 174: 9–22.
71. Albisetti GW, Ghanem A, Foster E, Conzelmann KK, Zeilhofer HU, Wildner H. Identification of two classes of somatosensory neurons that display resistance to retrograde infection by rabies virus. J Neurosci 2017, 37: 10358–10371.